

Optimised Multithreaded CV-QKD Reconciliation for Global Quantum Networks

Xiaoyu Ai and Robert Malaney

School of Electrical Engineering & Telecommunications,
University of New South Wales, Sydney, NSW 2052, Australia.

Abstract—Designing a practical Continuous Variable (CV) Quantum Key Distribution (QKD) system requires an estimation of the quantum channel characteristics and the extraction of secure key bits based on a large number of distributed quantum signals. Meeting this requirement in short timescales is difficult. On standard processors, it can take several hours to reconcile the required number of quantum signals. This problem is exacerbated in the context of Low Earth Orbit (LEO) satellite CV-QKD, in which the satellite flyover time is constrained to be less than a few minutes. A potential solution to this problem is massive parallelisation of the classical reconciliation process in which a large-code block is subdivided into many shorter blocks for individual decoding. However, the penalty of this procedure on the important final secured key rate is non-trivial to determine and hitherto has not been formally analysed. Ideally, a determination of the optimal reduced block size, maximising the final key rate, would be forthcoming in such an analysis. In this work, we fill this important knowledge gap via detailed analyses and experimental verification of a CV-QKD sliced reconciliation protocol that uses large block-length low-density parity-check decoders. Our new solution results in a significant increase in the final key rate relative to non-optimised reconciliation. In addition, it allows for the acquisition of quantum secured messages between terrestrial stations and LEO satellites within a flyover timescale even using off-the-shelf processors. Our work points the way to optimised global quantum networks secured via fundamental physics.

I. INTRODUCTION

Continuous Variable (CV) Quantum Key Distribution (QKD) has been intensively studied and significant breakthroughs have been achieved in both theory and experiment (see [1] for review). Compared to Discrete Variable (DV) QKD [2]–[5], CV-QKD can be implemented with well-developed technologies (e.g., homodyne detectors) in commercial fibre-optic networks [6], [7] and free-space optical communications [8], [9], providing it a potential advantage in practical deployments [10]–[14].

Considering the finite-key security of CV-QKD and DV-QKD, there are three critical parameters. These are, N_o , the number of original quantum signals sent by the transmitter (Alice) that are collected by the receiver (Bob); N_e , the number of quantum signals from which the protocol parameters are estimated;¹ and, ϵ , the probability that a QKD protocol fails to generate secret keys [15], [16]. To satisfy an upper limit on the failure probability of parameter estimation, Alice and Bob set N_e to a large value, which in turn implies a larger N_o .

Despite the advantages in deployment, CV-QKD systems tend to demand a larger N_o to reach the same ϵ relative to DV-QKD protocols. For example, to achieve a final key rate of 0.1 bits per pulse with $\epsilon = 10^{-9}$, a CV-QKD protocol studied in [17] required $N_o \approx 10^9$ signals. However, to achieve the same final key rate with $\epsilon = 10^{-14}$, the DV-QKD protocol in [18] required $N_o \approx 10^4$ signals. This higher number of required signals in CV-QKD can render the classical post-processing (i.e. key reconciliation and privacy amplification²) slow - possibly failing to meet target timescales for reconciliation.

The end-users of a CV-QKD system expect the system to deliver two identical and secure keys under a limited time interval. For example, for satellite-based deployments, we would hope that the reconciliation is completed while maintaining a line-of-sight connection with the ground station. For a CV-QKD-enabled satellite with orbital parameters similar to *Micius* [20], this would mean the reconciliation should be completed in less than a few minutes. For the protocol we use in this work (see later), and for $\epsilon = 10^{-9}$, this, in turn, would require the data rate of reconciliation to be at least 3.6×10^6 bits per second. For real-time reconciliation (say in sub-second timescales), two orders of magnitude increases in the reconciliation rates would be required. Demands for smaller ϵ will exacerbate the issue. Ideally, the rate of reconciliation should always be faster than the rate of quantum signalling.

This all raises the question as to whether current CV-QKD reconciliation schemes are optimised for the highest possible key rates in bits per second. As we show here, this is not the case. Further optimisation is possible on all current schemes.

To understand the issue better, we define reconciliation in the context of CV-QKD as a two-step scheme where the inputs to the reconciliation are non-identical $N = 2N_o - 2N_e$ quadrature values³ held by Alice and Bob (after parameter estimation), and the output is an identical bit string held by Alice and Bob [21]–[23]. Assuming a reverse reconciliation scheme, Bob first converts the quadrature values encoded by Alice in each signal to m bits. Alice, after converting each of her encoded real numbers also to m bits, then initiates some discrepancy-correction algorithms based on pre-defined error-correction codes to ensure her mN bits are identical to Bob's.

²In this work, we focus on the key reconciliation step because it is the more time-consuming part in the post-processing steps while the privacy amplification involving only bit-wise operations can be easily implemented faster than the reconciliation [19].

³ N_o and N_e are multiplied by 2 since Alice and Bob utilise both quadratures from heterodyne detection - the detection process we assume in this work.

¹More precisely, in a CV-QKD protocol, Alice and Bob randomly select a N_e -signal subset from the N_o signals to estimate the parameters.

In this work, we will adopt Low-Density Parity-Check (LDPC) codes for the error correction.

However, as alluded to above, reconciling mN bits within a limited time frame can be challenging. State-of-the-art LDPC-based reconciliation schemes for CV-QKD systems involve parallelised computation on a Graphics Processing Unit (GPU) [13], [24] or Field-Programmable Gate Arrays (FPGAs) [25], [26]. Reconciliation schemes implemented on FPGAs offer more programmable flexibility, but sometimes at the cost of reduced memory access relative to GPUs. For our purposes, both hardware architectures are useful - both offer massive parallelisation opportunities. These parallelisation solutions generally take the following two-step approach: 1) The mN bits are organised as m N -bit blocks to be reconciled. Each N -bit block is divided into multiple shorter blocks of size, say, N_R . This is usually just set to a block size that can be processed within some timescale. 2) Then the m N_R -bit blocks are reconciled in parallel (via independent processors) using optimally-designed LDPC decoders. However, what is missing in this approach is a proper optimisation analysis as to what the optimal value of N_R is. As we show below, simply reducing N_R at the cost of additional processing units is not an optimal solution. It transpires that in QKD the ‘‘penalty’’ cost of reducing the code rate (implicit in the use of small block lengths) significantly influences the bit per second final key rate.

A more sophisticated analysis is required to determine the optimal reduced block length. Such an analysis is the key contribution of this work. Although we will adopt a specific CV-QKD protocol for our analysis, the key steps of our scheme will apply to any CV-QKD protocol. Our reconciliation scheme will deliver the highest reconciliation rate for a given processor speed - thus allowing for the optimal solution to CV-QKD reconciliation.

II. SYSTEM OVERVIEW

Although, as just stated, our analysis will apply to most CV-QKD protocols, for detailed quantitative discussion we will consider only one specific CV-QKD protocol - the ‘‘no-switching’’ protocol [27]–[29] based on heterodyne detection. In this protocol, the quantum signal is encoded using Gaussian-modulated coherent states [27]. The main advantage of the no-switching protocol is that Alice and Bob can utilise all measurement results [28] (in most other protocols some results are discarded due to a random quadrature selection). We also adopt a Slice Reconciliation (SR) variant named Multi-Stage Hard Decoding⁴ (MSHD) [30], [33], [34] for the classical reconciliation step, where the number of bits derived from each measurement outcome is m . We refer to this variant simply as SR in the following.

⁴The slice reconciliation can be implemented with 2 other variants: Bit Interleaved Coded Modulation (BICM) [30] and Multi-Level Coding/Multi-Stage Decoding (MLC/MSD) [31], [32]. We note that the MLC/MSD takes advantage of the dependence between slices to select the optimal LDPC code rates [30], [32]. However, as a special case of MLC/MSD, MSHD assumes that the slices are independent [30], [33], [34]. Using MSHD leads to a tractable analysis at the expense of sub-optimal selection of LDPC code rates, but such expense is negligible if Gray Labelling [35] is adopted and the number of slices is at least 5 [30], [34], as is the case in this work.

It is worth noting that the optimisation analysis to follow is to some extent independent of the details of the reconciliation scheme. However, SR [30], [36] can be compared with the other well-known reconciliation scheme for CV-QKD - multidimensional reconciliation [37]. It is known that SR achieves higher reconciliation efficiency when the Signal-to-Noise Ratio (SNR) is greater than 1 [36]. At low SNR the opposite is true. For focus, here we adopt SR (as multistage hard decoding [36]) since in many satellite scenarios post-selection is used to filter out the low SNR quantum signals [1]. Our adopted scheme will be more useful in such scenarios.

We now briefly describe the steps of the protocol, a diagram of which shown in Fig. 1. In the following, we assume the quantum signalling rate is much larger than the reconciliation rate.

- **Step 1: Signal Preparation.** Alice selects a fixed modulation variance V_A . For each quantum signal to be transmitted to Bob, Alice randomly selects a number from a Gaussian distribution, $N(0, V_A)$, and then prepares a signal by displacing one of the quadrature components of a vacuum state by this random number. The process is repeated on the signal for the other quadrature. The signal is then transmitted to Bob.
- **Step 2: Heterodyne Detection.** Bob performs heterodyne detection to obtain the two quadrature values (real numbers) for each received signal. Bob compares each measured quantum signal with a given cut-off threshold and informs Alice to discard her corresponding quantum signal if his measured quantum signal is lower than the threshold⁵. A quantum signal that is lost in transit registers a null signal at Bob. Neglecting null signals, Bob holds $2N_o$ quadrature values at the end of this process.
- **Step 3: Parameter Estimation.** Bob randomly selects a subset $2N_e$ from the $2N_o$ quadrature values and sends this *estimation subset*, along with the corresponding time information, to Alice via classical communications (we adopt $N_e = \frac{1}{2}N_o$, unless otherwise stated). Alice uses the timing information to best pair the signals in this subset (and therefore the corresponding quadrature values) sent by her and then estimates the covariance matrix between the shared states. Based on the estimated covariance matrix, Alice determines the channel transmissivity, T , excess noise, ξ , Bob’s SNR, γ , the Holevo Information, χ_{BE} , between Bob and the eavesdropper (Eve), and the mutual information between Alice and Bob, I_{AB} . Finally, for a given target reconciliation efficiency β , Alice compares χ_{BE} with βI_{AB} . Alice aborts the protocol if $\chi_{BE} \geq \beta I_{AB}$. Otherwise, Alice informs Bob of the estimation results, i.e. T , ξ , γ , χ_{BE} and I_{AB} .
- **Step 4: Bit Error Estimation for SR.** Using Gray Labelling, Alice and Bob represent each of the quadrature values embedded in each signal with m bits. Then, for quadrature values selected in the estimation subset, Alice forms a N_e -by- m bit matrix and Bob does the same. Next,

⁵The Gaussian post-selection technique at Bob’s side effectively improves the channel conditions between Alice and Bob [38] so that SR is preferred for reconciliation (rather than multidimensional reconciliation).

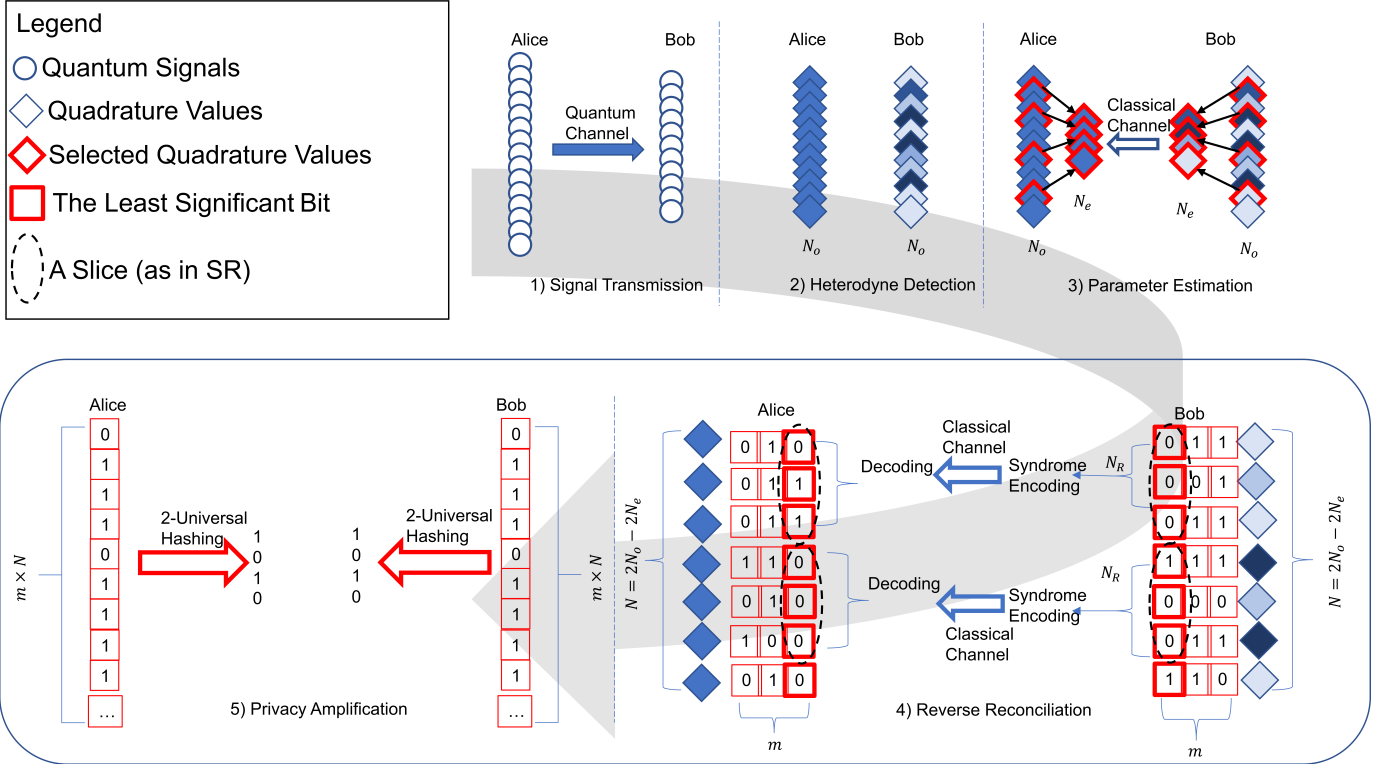


Fig. 1: Diagram of the reconciliation. 1) Alice prepares and sends Gaussian-modulated coherent states to Bob during the signal transmission. 2) Bob performs heterodyne detection to obtain quadrature values. Blue diamonds at Alice’s side represent Alice’s quadrature values. Diamonds filled with tinted or shaded blue at Bob’s side show that his quadrature values deviate from what was prepared by Alice after transmission. 3) Alice and Bob select and exchange a random subset of the quadrature values (diamonds with red outlines) to perform parameter estimation. 4) Alice and Bob perform reverse reconciliation based on SR to convert their quadrature values into two bit strings and reconcile them. 5) Alice and Bob perform privacy amplification to obtain two identical but shorter key strings about which Eve has effectively no knowledge.

Alice and Bob exchange their matrices and compare the j^{th} column of the two matrices to estimate the Bit Error Ratio⁶ (BER), $p_j, j \in \{0, 1, \dots, m-1\}$, for all the digits in the j^{th} column. The estimated p_j will be used in SR. Finally, Alice and Bob discard all the quadrature values in the estimation subset. At the end of this step, Alice and Bob each hold a mN -bit string.

- **Step 5: Reverse Reconciliation.** For each column, Alice and Bob agree on an LDPC code with block length N_R that is closest to the capacity determined by p_j . Bob forms a new N_R -bit string (referred as a “slice” in SR) by selecting the j^{th} digit (bit) of each of the N_R quadrature values, encodes the new bit string (the slice) into syndrome bits, and sends those bits to Alice (see III.B for details). Alice then initiates SR to obtain her best estimate of Bob’s string. Alice repeats this process until all her mN bits are reconciled. Finally, Alice and Bob obtain two hashed strings by applying the same hash function to their reconciled strings and exchange the hash results to check whether SR is successful. If successful, Alice holds a mN -bit string identical to Bob’s mN -bit string. Otherwise, they abort the protocol and restart from

⁶At this step, sources of bit errors include the channel transmission, heterodyne detection, and quantisation.

Step 1.

- **Step 6: Privacy Amplification.** Based on Eq. 19, Alice and Bob compute the length of the secret key that can be extracted and then apply a 2-universal hashing function on their reconciled string to obtain two identical and shorter secret key strings about which Eve has effectively no knowledge.

III. OVERCOMING THE LIMITATIONS OF KEY RECONCILIATION

A. GPU-based SR

The process of SR is to reconcile mN bits. One can naively use m LDPC matrices with $N_R = N$ for each matrix. However, due to practical hardware limitations, the process is better implemented by dividing N into N_d blocks of some smaller N_R so that the same LDPC decoders can reconcile these blocks in parallel. This process resembles the idea of *Single Program Multiple Data* (see [39], [40] for more details). As illustrated in Fig. 2, we implement SR by creating N_d LDPC decoders loaded with the same LDPC matrix on N_d GPU threads and let these decoders reconcile N_d blocks in parallel. This helps to reduce the SR timescale and assists in meeting the time constraints, such as those posed in satellite-

based scenarios. Section V-A will demonstrate in detail the advantage of using such parallelisation.

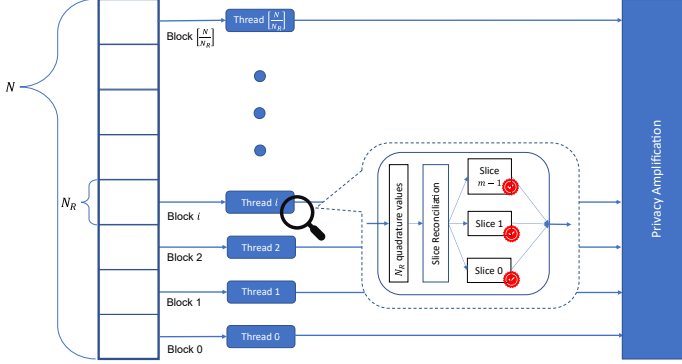


Fig. 2: Diagram of GPU-based SR adopted in this work. N quadratures values are divided into multiple blocks of length N_R . Each block is loaded to one thread that is dedicated to performing SR for this block. The reconciled bits obtained from each thread are collected and ready for privacy amplification. The floor operator is shown as $\lfloor \cdot \rfloor$.

B. The Penalty of Using Finite-Length LDPC Codes

An illustration of the SR scheme is shown in Fig. 3. The generic steps are: 1) for the i^{th} quadrature value, $y^i, i = 0, 1, \dots, N_R - 1$, Bob applies a constant-step quantisation function, $M(\cdot)$, to convert y^i to an m -bit string⁷ denoted as $\{l_0^i, l_1^i, \dots, l_{m-1}^i\}$, where $l_j^i, j = 0, \dots, m - 1$ is the binary bit for the j^{th} digit of the i^{th} quadrature value. 2) We define that the j^{th} slice, \mathbf{S}_j , is a bit string with length N_R created by Bob: $\mathbf{S}_j = \{l_j^0, l_j^1, \dots, l_j^{N_R-1}\}$. For \mathbf{S}_j , Bob applies an LDPC matrix, H_j based on p_j obtained in parameter estimation to obtain the corresponding syndrome bits. 3) Bob sends Alice the syndrome bits of \mathbf{S}_j and H_j via classical communications. 4) Alice uses her quadrature values as side information and what was transmitted by Bob as the inputs of the LDPC decoder. Alice takes the soft decoding output (the log-likelihood ratio when the decoding finishes) of \mathbf{S}_{j-1} as the input to accelerate the reconciliation of \mathbf{S}_j (except for \mathbf{S}_0)⁸ [30], [41]. 5) Alice obtains her estimated version of \mathbf{S}_j . Then, Alice and Bob move on to \mathbf{S}_{j+1} . 6) Alice and Bob repeat Step 1 to 5 until all N values are reconciled. We note that Alice and Bob use m LDPC matrices to reconcile m slices in a block - but the same m LDPC matrices are used for reconciling all N_d blocks since the quantisation errors are the same for a given m [42].

In SR, Bob needs to transmit syndrome bits to Alice based on the selected LDPC matrix with the code rate, R_j , for \mathbf{S}_j via classical communications. For a given channel condition, selecting R_j closest to the capacity is the common approach to minimise the number of bits disclosed to the eavesdropper while Alice can still reconstruct Bob's quantised bits without

error [36]. Specifically, for a given T , we can obtain the SNR, γ , as [42]

$$\gamma = \frac{\frac{1}{2}V_A T}{1 + \frac{1}{2}\xi}, \quad (1)$$

where V_A is the modulation variance at Alice side, $\xi = \xi_{ch} + \xi_d$ is the total noise power, ξ_{ch} is the channel excess noise, and ξ_d is the detector noise. Finally, the reconciliation efficiency $\beta \in [0, 1]$ for the SR is obtained via [31]

$$\beta = \frac{\Pi(M(Y)) - m + \sum_{j=0}^{m-1} R_j}{I_{AB}}, \quad (2)$$

where Y is a vector of Bob's quadrature values of length N_R , $M(Y)$ is a mN -bit string obtained by applying the quantisation function $M(\cdot)$ to each quadrature value in Y , and $\Pi(M(Y))$ is the entropy function of $M(Y)$. Increasing m to values that render the quantisation error negligible is always possible, but this would require the individual LDPC codes for every j^{th} slice to be near perfect (capacity-achieving) otherwise the efficiency β will be low; $m = 5$ is found to be a good pragmatic compromise, and is adopted here. Given five slices a constant quantisation size of the real line across 2^5 bins centered on zero is chosen. This size, which is dependent on the adopted γ , optimises β (see [31] for further discussion).

The LDPC code rates, R_j , in Eq. 2 are the actual rates of the specific codes used for each slice (of length N_R). Normally, in practice, N_R is simply set to some value that allows target time-frames to be met, given that the decoding time is an increasing function of the block length [24]. We use R_j to obtain our experimental key rate in Eq. 32. A more nuanced value of that N_R that optimises secure key rates is now analysed.

To make progress in our task, we utilise a previous analysis of channel coding in the finite block-length [43] regime as a means to further investigate the effective channel capacity, C_{Finite} for a given block length N_R and γ . For a finite message set \mathcal{M} , C_{Finite} is the ratio of the maximum size of \mathcal{M} that can be transmitted via N_R channel uses with a decoding error probability less than ϵ_{EC} . Specifically, for an Additive White Gaussian Noise Channel (AWGNC), C_{Finite} is given by⁹ [43]

$$C_{Finite} \approx C(\gamma) - \frac{\sqrt{N_R A} Q^{-1}(\epsilon_{EC}) + \frac{1}{2} \log N_R}{N_R}, \quad (3)$$

where $C(\gamma) = \frac{1}{2} \log(1 + \gamma)$ is the Shannon Capacity for the given γ , $Q^{-1}(s)$ is the inverse of the Q-function

$$Q(z) = \frac{1}{\sqrt{2\pi}} \int_z^\infty e^{-\frac{t^2}{2}} dt, \quad (4)$$

and A is given by

$$A = \frac{\gamma}{2} \frac{\gamma + 2}{(\gamma + 1)^2} (\log \epsilon_{EC})^2. \quad (5)$$

Function A is termed the ‘‘channel dispersion’’ since it represents the reduction of the code rate from the channel capacity due to a tolerated decoding error probability. It is the ‘‘price

⁷We assume the least significant bit is l_0^i .

⁸The rationale behind this is that the soft decoding output of \mathbf{S}_{j-1} provides *a priori* information on the reliability of each bit in \mathbf{S}_j [30].

⁹This approximation is accurate if the code achieves more than 80% of the capacity [43].

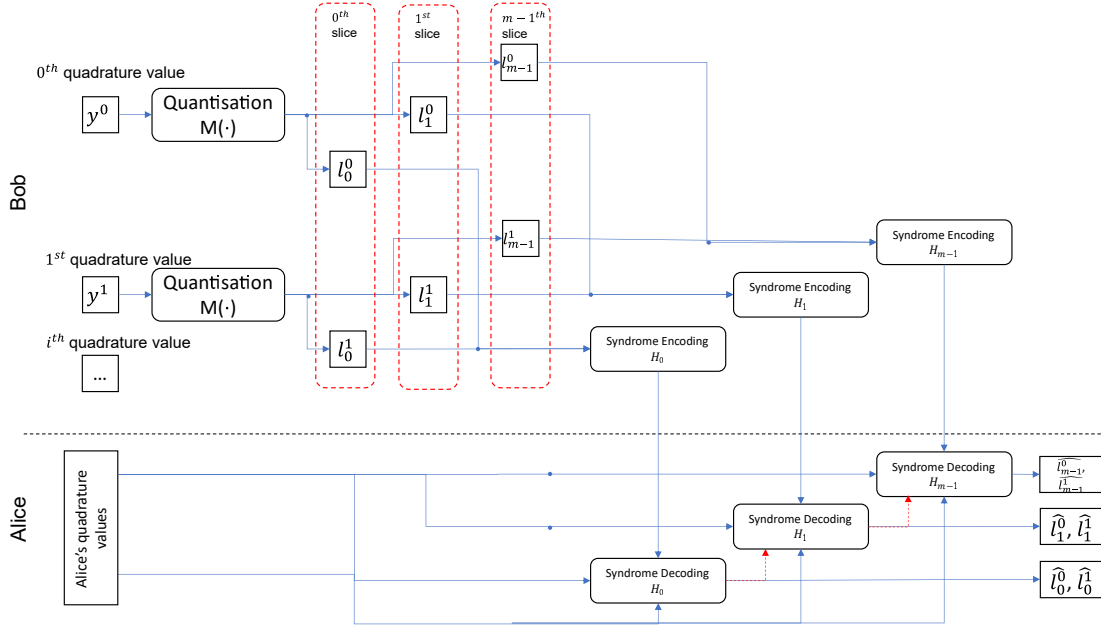


Fig. 3: Diagram of SR. The red dashed arrows show the soft decoding output feeds from S_{j-1} to S_j . The red dashed rectangles are graphical examples of a slice.

to pay” for using a code with finite block length, for a given γ .

Note, C_{Finite} is the upper bound of $\sum_{j=0}^{m-1} R_j$ for a given ϵ_{EC} and N_R . To simplify the determination of the code rate in the finite-length regime, we determine C_{Finite} instead of each R_j for the purpose of analysis. Using Eq. 3 we introduce β_{Finite} as an analytical reconciliation efficiency in the finite LDPC block length regime (neglecting the information loss due to the quantisation process). This is given by

$$\beta_{Finite} = \frac{C_{Finite}}{I_{AB}} \approx \frac{I_{AB} - \frac{\sqrt{N_R} A Q^{-1}(\epsilon_{EC}) + \frac{1}{2} \log N_R}{N_R}}{I_{AB}}. \quad (6)$$

Eq. 6 explicitly illustrates how LDPC codes with long block lengths generally reduce the information disclosed to Eve during reconciliation.

We demonstrate the connection between β_{Finite} and β . Firstly, we rewrite Eq. 2 as

$$\beta = \frac{\Pi(M(Y)) - R_s}{I_{AB}}, \quad (7)$$

where $R_s = \sum_{j=0}^{m-1} (1 - R_j) = m - \sum_{j=0}^{m-1} R_j$ is the ratio of syndrome bits sent by Bob to the total number of bits in m slices. R_s is the side-information that Alice uses to reconcile her m slices [32]. It is known that R_s satisfies the SlepianWolf Bound [44]

$$R_s \geq \Pi(M(Y)|X), \quad (8)$$

where X is a vector of Alice’s quadrature values of length N_R . Applying Eq. 8 to Eq. 7, we have

$$\frac{\Pi(M(Y)) - R_s}{I_{AB}} \geq \frac{\Pi(M(Y)) - \Pi(M(Y)|X)}{I_{AB}} = \frac{I(M(Y); X)}{I_{AB}}, \quad (9)$$

where $I(M(Y); X)$ is the total mutual information (after quantisation) between Alice and Bob. Recalling that C_{Finite} is the upperbound of the mutual information between Alice and Bob for an LDPC block length, we have the following

$$1 \geq \beta \geq \frac{I(M(Y); X)}{I_{AB}} \geq \frac{C_{Finite}}{I_{AB}} = \beta_{Finite} \geq 0. \quad (10)$$

C. Analysing the Computational Complexity of SR

An LDPC matrix with block length N_R can be defined by the symbol and check node degree distribution polynomials, $\lambda(x) = \sum_{a=2}^{\Lambda} \lambda_a x^{a-1}$ and $\rho(x) = \sum_{b=2}^P \rho_b x^{b-1}$. Here, Λ and P are the highest degrees in $\lambda(x)$ and $\rho(x)$, respectively. We denote the total number of non-zero entries in an LDPC matrix as G , and adopt the well-known Belief Propagation (BP) decoder [45] for error correction. We define the total number of arithmetic operations of SR as $\sum_{j=0}^{m-1} E_j D_j$, where, for each S_j , E_j is the number of arithmetic operations executed within a decoding iteration,¹⁰ and D_j is the number of decoding iterations [46]. We note, in our GPU-based SR, E_j and D_j are different for the m slices of each block since m LDPC matrices are used to reconcile the m slices. For a channel with constant T and ξ , D_j is dependent on a target ϵ_{EC} , and on the polynomials $\lambda(x)$ and $\rho(x)$. Note, for N_R larger than approximately 10^5 , D_j is independent of N_R (a result we will adopt later). Assuming the Gaussian approximation within the Density Evolution Algorithm, D_j is given by

$$D_j = \arg \min_k \{q_k = f(\gamma, k, \lambda(x), \rho(x)) \leq \epsilon_{EC}, k \in \mathbb{Z}^*\}, \quad (11)$$

¹⁰In a BP decoder, a decoding iteration is one pass through the decoding algorithm.

where q_k is the BER after the k^{th} decoding iteration and given by [47]

$$\begin{aligned} q_k &= f(\gamma, k, \lambda(x), \rho(x)) \\ &= \sum_{b=2}^P \rho_b \phi^{-1}(1 - L^{b-1}). \end{aligned} \quad (12)$$

Here

$$L = 1 - \sum_{a=2}^{\Lambda} \lambda_a \phi(\log \gamma + (a-1)q_{k-1}), \quad (13)$$

where $q_0 = 0$, and $\phi(v)$ is given by

$$\phi(v) = \begin{cases} 1 - \frac{1}{\sqrt{4\pi v}} \int_{-\infty}^{+\infty} \tanh\left(\frac{u}{2}\right) e^{-\frac{(u-v)^2}{4v}} du & v > 0 \\ 1 & v = 0. \end{cases} \quad (14)$$

Finding a closed solution to Eq. 12 is problematic due to the $\phi^{-1}(w)$ term (here $w = \phi(v)$). To make progress, the following approximation for Eq. 14 is used [47]

$$\phi(v) \approx \begin{cases} e^{-0.4527v^{0.86} + 0.0218} & v > 0 \\ 1 & v = 0. \end{cases} \quad (15)$$

We then find $\phi^{-1}(w)$ is given by

$$\phi^{-1}(w) \approx \begin{cases} \left(\frac{\log w - 0.0218}{-0.4527}\right)^{1.1628} & 0 < w < 1 \\ 0 & w = 1. \end{cases} \quad (16)$$

With this all in place, it is now possible to solve for D_j as given by Eq. 11.

Now we focus on the determination of E_j . When messages are propagated from the variable nodes to the check nodes, there are $2G$ multiplications and G additions [48]. When messages are propagating back to the variable nodes, there are $4G$ operations required ($2G$ multiplications and $2G$ additions) [48]. Therefore, E_j is obtained by [46], [48]

$$\begin{aligned} E_j &= 7G \\ &= 7N_R \left(\frac{\sum_{b=2}^P \frac{\rho_b}{b}}{\sum_{a=2}^{\Lambda} \frac{\lambda_a}{a}} \right) \left(\sum_{b=2}^P b \rho_b \right). \end{aligned} \quad (17)$$

The decoding time of the whole reconciliation process, Δt , is given by

$$\Delta t = c_h \sum_{j=0}^{m-1} E_j D_j, \quad (18)$$

where c_h is a hardware-dependent constant representing the time taken to complete an arithmetic operation. Clearly, by dividing N values into multiple blocks with length N_R and decoding these blocks simultaneously, Alice and Bob can reduce the decoding time by a factor of $N_d = \frac{N}{N_R}$.

IV. FINAL KEY RATE

We now present the penalty incurred for the division of N in the finite-key regime, and then propose an optimisation procedure to find the optimal N_R which maximises the final key rate in bits per second.

A. Analysis of the Final Key Rate

For the protocol considered, in the finite-key regime the final key rate in bits per pulse, K , under the assumption of Gaussian collective attacks is adopted as [28], [49], [50]¹¹

$$K = \frac{N(\beta I_{AB} - S_{BE}^{\epsilon_{PE}}) - \sqrt{N} \Delta_{AEP} - 2 \log_2 \frac{1}{2\epsilon_{PA}}}{N_o}, \quad (19)$$

where $S_{BE}^{\epsilon_{PE}}$ is the upper bound of the estimated χ_{BE} (note K is an upper bound, which we assume is reached). The determination of $S_{BE}^{\epsilon_{PE}}$ is carried out and utilised in the key rates derived here, but this determination is somewhat lengthy. As such, the reader is referred to the appendix for a full explanation and derivation of this term. We simply note here that $S_{BE}^{\epsilon_{PE}}$ is dependent on estimates of the channel parameters and therefore on the value of N_e , the number of symbols sacrificed in the estimation. In Eq. 19, Δ_{AEP} is a penalty term (derived using the Asymptotic Equipartition Property of a stochastic source) due to the finite number of bits used in quantisation and privacy amplification, and is given by

$$\begin{aligned} \Delta_{AEP} &= (m+1)^2 + 4(m+1) \sqrt{\log_2 \left(\frac{2}{\epsilon_s^2} \right)} \\ &\quad + 2 \log_2 \left(\frac{2}{\epsilon_s^2 \epsilon_s} \right) + \frac{4\epsilon_s m}{\epsilon \sqrt{N}}, \end{aligned} \quad (20)$$

where $\epsilon = \epsilon_{EC} + 2\epsilon_s + \epsilon_{PA} + \epsilon_{PE}$ is the probability that a QKD protocol fails to generate secret keys. Here, ϵ_s is the smoothing parameter associated with the smooth min-entropy calculation, ϵ_{PA} is the failure probability of the privacy amplification, and ϵ_{PE} is the probability that the true value of χ_{BE} is not within the confidence interval calculated during parameter estimation. For a given ϵ , one can determine the values of ϵ_{EC} , ϵ_s , ϵ_{PA} , and ϵ_{PE} by setting them individually or collectively as part of the maximisation of K (see Eqs. 18 – 21 in [17] for details).

We consider the penalty on the final key rate caused by dividing N into sub-blocks of length N_R . Replacing β in Eq. 19 with the β_{Finite} of Eq. 6, we obtain the final key rate with the finite LDPC block length effect fully considered. The new rate is given by

$$K_{Finite} = \frac{N(C_{Finite} - S_{BE}^{\epsilon_{PE}}) - \sqrt{N} \Delta_{AEP} - 2 \log_2 \frac{1}{2\epsilon_{PA}}}{N_o}. \quad (21)$$

Thus far, we have been analysing the final key rate in bits per pulse. However, the final key rate in bits per second is more interesting in our context - the system will not be viable if the reconciliation takes too long to complete. From this point forward, we use a dashed symbol to distinguish a final key rate that is given in bits per second. Taking the decoding complexity into account, and ignoring the time taken to acquire

¹¹This key-rate formulation was developed in [49] with a typographical error corrected in [50]. Eq. 19 is from [28] which acknowledged the correction and simplified the final key rate formulation (see footnote 2 of [51] for more details). A general discussion on the use of other key-rate formulations (e.g. [52], [53]) within our framework is given later.

the quantum signals, we can write the final key rate, K'_{Finite} , as

$$\begin{aligned} K'_{Finite} &= \frac{N_o K_{Finite}}{\Delta t} \\ &= \frac{N(C_{Finite} - S_{BE}^{\epsilon_{PE}}) - \sqrt{N}\Delta_{AEP} - 2 \log_2 \frac{1}{2\epsilon_{PA}}}{c_h \sum_{j=0}^{m-1} E_j D_j}. \end{aligned} \quad (22)$$

We observe that Δt in Eq. 18 and C_{Finite} in Eq. 3 are increasing functions of N_R . We are interested in finding a unique N_R so that K'_{Finite} is maximised.

B. Optimised LDPC Blocklength for CV-QKD Reconciliation

Previously, we have shown that parallelisation reduces the decoding time at the expense of increased information disclosure to Eve. In this section, we demonstrate an optimisation process to find the unique N_R maximising K'_{Finite} .

We consider a scenario where ϵ_{EC} , ϵ_s , ϵ_{PA} , and ϵ_{PE} are manually set by end users. We can formulate the optimisation problem for the scenario

$$\begin{aligned} \max_{N_R} \quad & K'_{Finite} \\ \text{s.t.} \quad & 10^5 \leq N_R \leq N, \end{aligned} \quad (23)$$

where K'_{Finite} is defined in Eq. 22. The lower limit of 10^5 arises from our earlier discussion on ensuring D_j is independent of N_R (for smaller values of N_R the penalty cost will be prohibitive and we ignore this range). We notice that Δt is a linear function of N_R ¹² and $S_{BE}^{\epsilon_{PE}}$; and that Δ_{AEP} and ϵ are independent of N_R . Therefore, we can rewrite Eq. 23 in the simplified form

$$\begin{aligned} \max_{N_R} \quad & \frac{NC_{Finite} - B_1}{B_2 N_R} \\ \text{s.t.} \quad & 10^5 \leq N_R \leq N, \end{aligned} \quad (24)$$

where

$$B_1 = NS_{BE}^{\epsilon_{PE}} + \sqrt{N}\Delta_{AEP} + 2 \log_2 \frac{1}{2\epsilon_{PA}}, \quad (25)$$

$$B_2 = \sum_{j=0}^{m-1} 7 \left(\frac{\sum_{b=2}^P \frac{\rho_b}{b}}{\sum_{a=2}^P \frac{\lambda_a}{a}} \right) (\sum_{b=2}^P b \rho_b) D_j c_h. \quad (26)$$

To solve this optimisation problem, firstly we show that the second derivative of K'_{Finite} with respect to N_R is less than zero for all N_R considered, where

$$\begin{aligned} \frac{d^2 K'_{Finite}}{dN_R^2} &= \frac{-1}{4B_2 N_R^4} ((12N \log N_R - 10N) \\ &\quad + 15\sqrt{AQ}^{-1}(\epsilon_{EC})N\sqrt{N_R} \\ &\quad - (8I_{AB}NN_R - 8B_1N_R)). \end{aligned} \quad (27)$$

To show that the RHS of Eq. 27 is less than zero for all N_R considered, it is equivalent to show

$$\begin{aligned} 12N \log N_R - 10N + 15\sqrt{AQ}^{-1}(\epsilon_{EC})N\sqrt{N_R} \\ > (8I_{AB}NN_R - 8B_1N_R). \end{aligned} \quad (28)$$

We find that the LHS of inequality 28 is greater than zero for $N > N_R > 10$, $\gamma > 0$, and $\epsilon_{EC} < \frac{1}{2}$, but the

¹²Recalling Eq. 18, we note that for a given LDPC code, E_j is only dependent on the degree distribution pairs and D_j is only a function of the degree distribution pairs and γ .

sign of the RHS is subject to specific CV-QKD parameters. However, through detailed numerical search we find that the inequality 28 holds for the range of parameters anticipated for realistic CV-QKD deployments.¹³ For example, if we consider the following CV-QKD settings¹⁴ (in the following we refer to these as the standard CV-QKD settings); $N = 10^9$, $m = 5$, $\epsilon_{EC} = 2\epsilon_s = \epsilon_{PA} = \epsilon_{PE} = 2.5 \times 10^{-10}$, $V_A = 5$, $T = 0.9$, $\xi_{ch} = 0.0186$ and $\xi_d = 0.0133$, we find that the LHS of the inequality is greater than 10^{12} and the RHS of the inequality is less than 10^{11} .

To find the maximised K'_{Finite} , we first find the value of N_R that satisfies $\frac{dK'_{Finite}}{dN_R} = 0$, where

$$\begin{aligned} \frac{dK'_{Finite}}{dN_R} &= \frac{N_R N \frac{dC_{Finite}}{dN_R} - (NC_{Finite} - B_1)}{B_2 N_R^2} \\ &= -\frac{NI_{AB}}{B_2 N_R^2} - \frac{N}{2B_2 N_R^3} + \frac{3N\sqrt{AQ}^{-1}(\epsilon_{EC})}{2B_2 N_R^{\frac{5}{2}}} \\ &\quad + \frac{N \log N_R}{B_2 N_R^3} + \frac{B_1}{B_2 N_R^2}. \end{aligned} \quad (29)$$

Therefore, our equation to be solved is given by

$$-\frac{NI_{AB}}{B_2 N_R^2} - \frac{N - 2N \log N_R}{2B_2 N_R^3} + \frac{3N\sqrt{AQ}^{-1}(\epsilon_{EC})}{2B_2 N_R^{\frac{5}{2}}} + \frac{B_1}{B_2 N_R^2} = 0. \quad (30)$$

Eq. 30 can be solved via a numerical root-finding algorithm [54]. If we consider the standard CV-QKD settings, we obtain a stationary point at $N_R = 3.6 \times 10^7$ bits (the value of K'_{Finite} at this N_R is discussed later).

In closing this section we note the following in regard to alternate key-rate equations. Although we have adopted a specific CV-QKD protocol and specific key rate equation, different security analyses of our adopted protocol, and analyses of different CV-QKD protocols, can have a key rate with a similar form to that shown in Eq. 19 albeit with different bounded rates. When comparing different key-rate equations it is perhaps useful to only consider the leading terms. This allows for clearer tractability in determining the optimal N_R . For example, if the last term in our Eq. 20 is neglected (a good approximation for reasonable N values) then the functional dependence on N of many key-rate equations is identical. In such circumstances, the same key rate can be mapped to alternate security settings of the different key-rate equations, and our framework applies directly. For example, using the key rate equation of [52] we find the same optimal N_R albeit with a normalised key rate of one for the following security settings (described with the notations in [52]): the number of quantum signal exchanged, $N = 10^9$, the number of quantum signals sacrificed for parameter estimation, $m = \frac{N}{2}$, the probability of successful reconciliation, $p_{ec} = 0.95$, the smoothing parameter, $\epsilon_s = 3.2 \times 10^{-13}$, the hashing parameter

¹³In using this technique it is important to check that the inequality holds for the chosen parameter range of interest. This is done for all calculations we show here, but also for a much wider range not shown. For example, we find for $\epsilon = 10^{-9}$, $N = 10^9$ and $m = 5$, the inequality 28 holds for any combination of the remaining parameters selected from the ranges $V_A \in [1, 34]$, $T \in [0, 1]$ and $\xi = [0, 0.05]$.

¹⁴The values of ξ_{ch} and ξ_d in the standard CV-QKD settings are predicted values after accounting for all noise terms [17].

$\epsilon_h = 4.7 \times 10^{-13}$, the probability that the true value of the square-root transmissivity is less than the value obtained by the worst-case estimator used in parameter estimation, $\epsilon_{pe} = 1.2 \times 10^{-13}$, the residue probability that Alice and Bob's bit strings are different after passing the error correction, $\epsilon_{cor} = 0.8 \times 10^{-13}$, the modulation variance, $\sigma_x^2 = 7.1$, the size of the effective alphabet after quantising the continuous quadrature values, $d = 2^5 = 32$, the channel transmissivity, $T = 0.81$, the channel noise $\sigma_z^2 = 0.035$, and the quantum duty to pay by the detector, $\nu_{det} = 2$ for heterodyne detection. Key-rate equations with different functional dependence on N_R can still be analysed within the framework proposed here - albeit via modified optimisation relations. Examples of this arise in consideration of DV-QKD protocols (albeit for which reconciliation optimisation is usually less important). We also note that extension of our adopted CV-QKD key-rate equation, to cover the most general attack, is possible via the use of the Gaussian de Finetti reduction technique and the inclusion of an energy test [55]. This leads to a scaling of order N^4 in terms of the security cost.

V. EXPERIMENTAL RESULTS

We conducted an experiment of our GPU-based SR on a NVIDIA GTX 1060 GPU (with 6GB GPU memory). The GPU provides up to 1280 Compute Unified Device Architecture (CUDA) threads that can be run simultaneously. We determine the BER after decoding, denoted as p_{Decode} (different from the p_j obtained at Step 5 of the protocol). We also measured the decoding time for mN bits. Below, we determine the experimental final key rate, K'_{exp} , and compare it with K'_{Finite} to verify the optimality of N_R found in Section IV-B. We note that the experimental data shown in Figs. 4, 5, and 6 is averaged over 50 runs. We also note, in our specific GPU the number of threads available was less than the number of blocks when $N_R = 10^5$. This was numerically compensated for in the results shown.

In the experiment, we assume that Alice and Bob complete the first four steps of the protocol described in Section II. Since Alice and Bob's quadrature values are the input and output of an AWGNC, we can generate these quadrature values for SR in the following way. 1) For a given V_A , T , and ξ , we obtain the noise power, σ_n^2 of the AWGNC from Eq. 1

$$\gamma = \frac{\frac{1}{2}V_A T}{1 + \frac{1}{2}\xi} = \frac{1}{\frac{1 + \frac{1}{2}\xi}{\frac{1}{2}V_A T}} = \frac{1}{\sigma_n^2}. \quad (31)$$

2) We generate N random numbers from the distribution $N(0, V_A)$. These numbers are regarded as Alice's quadrature values and denoted as $\mathbf{x} = \{x_0, x_1, \dots, x_{N-1}\}$. 3) We obtain Bob's quadrature values \mathbf{y} , where the i th component is given by $y_i = x_i + n$, and where n is a random real number drawn from $N(0, \sigma_n^2)$.

A. Decoding Error and Time

In Fig. 4, we compare the BER performance of different N_R settings for each T considered¹⁵. The solid lines represent the best straight-line fit of the experimental data for each N_R . We note that for a given T , the LDPC code rates are set to 10% lower than the capacity for that T . In Fig. 4, we observe that larger LDPC codes lead to a lower p_{Decode} . This observation is consistent with the result of the finite-length information theory [43].

In Fig. 5, we determine the measured decoding time for mN bits in the experiment, Δt_{exp} , which is normalised to the value at $N_R = 10^9$ ($\Delta t_{exp} = 310$ seconds). The differences of the measured decoding time at each N_R reflect additional decoding iterations. Our results confirm the reduction of Δt_{exp} when a smaller N_R is used. We note that it is difficult to quantify the exact relation between Δt_{exp} and N_R since Δt_{exp} includes the elapsed time taken by SR's arithmetic operations and the elapsed time for the overhead; mostly due to memory access operations and synchronisation (we estimate this shortly). However, our experiment generally confirms the advantage of parallelisation in decoding time.

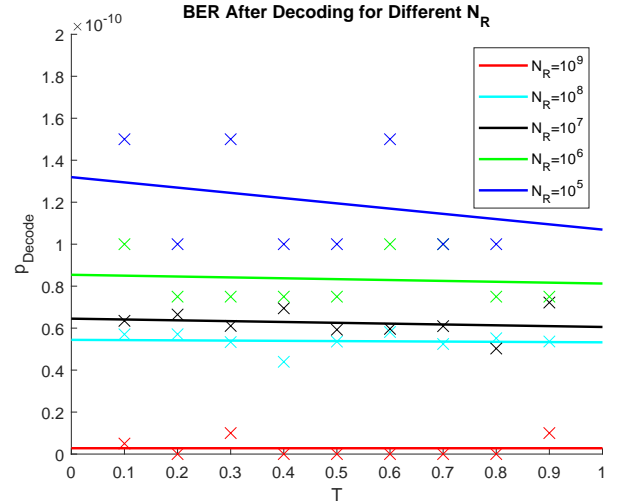


Fig. 4: p_{Decode} after decoding for different T and N_R . For each colour, the crosses are the experimental data obtained.

B. The Optimal N_R

Previously, we have analytically found the optimal N_R which maximises K'_{Finite} . Now we wish to check the compatibility of this N_R with the value that maximises K'_{exp} based on realistic LDPC codes and the specific GPU used in our experiment.

¹⁵Recall, we are particularly interested in the satellite-to-Earth channel. As in other works, we assume losses for this channel are dominated by diffraction effects, and therefore the transmissivity can be held constant. We further assume post-selections, using a bright classical beam sent along with the quantum signals (but different polarisation), remove any significant transmissivity deviations. As discussed elsewhere [17], some receiver/transmitter apertures, coupled to detailed phase-screen simulations of satellite downlink channels, render the constant-transmissivity assumption reasonable [56]. If the transmissivity is highly variable the optimal block length, N_R , can be calculated by an expectation over the transmissivity density function.

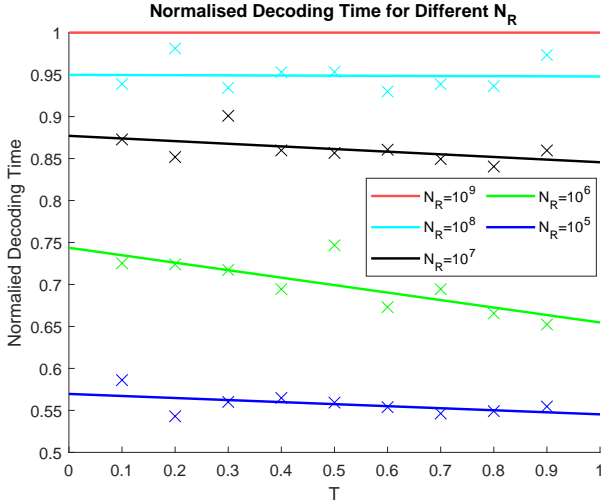


Fig. 5: Normalised decoding time vs. T for different N_R . For each colour, the crosses are Δt_{exp} obtained in our experiment. For each T , the data presented is the ratio of Δt_{exp} for each N_R to the decoding time for $N_R = 10^9$. The advantage offered by GPU parallel processing is seen to improve decoding times by $\sim 30\%$ for sub-blocks of length 10^6 .

For this experiment, we pre-built a database to store LDPC codes with their code rates ranging from 0.01 to 0.8 and their block lengths ranging from 10^6 to 10^9 . For code rates less than 0.1, Multi-Edge-Type LDPC codes (degree distributions outlined in [22]) were used. These achieve a lower p_{Decode} compared to irregular LDPC codes with the same code rate. For code rates greater than or equal to 0.1, we adopted the irregular LDPC codes (degree distributions outlined in [57]). At such code rates, these latter codes have the same p_{Decode} performance as the Multi-Edge-Type counterparts, but allow for faster code construction.

We use the following process to obtain K'_{exp} for each N_R considered. 1) For each S_j , we select an LDPC code whose code rate is closest to the capacity determined by p_j from the pre-built database. 2) We use the selected code to test whether the probability of an error correction failure of that code is less than ϵ_{EC} . 3) If the test fails, we decrease R_j by $\Delta R = 0.05$, select another LDPC code from the database and go back to Step 2). Otherwise, we mark the selected code as “good” and then go back to Step 1) for the next slice. The process terminates when all slices have been successfully decoded. We then obtain K'_{exp} using

$$K'_{exp} = \frac{N(\sum_{j=0}^{m-1} R_j - S_{BE}^{\epsilon_{PE}}) - \sqrt{N}\Delta_{AEP} - 2 \log_2 \frac{1}{2\epsilon_{PA}}}{\Delta t_{exp}}. \quad (32)$$

We note that the overhead mentioned earlier is one of the sources causing the discrepancy between K'_{exp} and K'_{Finite} . To compensate the additional decoding time due to the overhead for all N_R considered, we adopt a numerical search for a compensated Δt_{exp} so that $|K'_{exp} - K'_{Finite}|^2$ is minimised. Our result shows that K'_{exp} after compensation is approximately 10% higher than the uncompensated K'_{exp} . In Fig. 6,

we plot K'_{Finite} and K'_{exp} (compensated and uncompensated) with respect to N_R based on Eqs. 22 and 32, respectively.

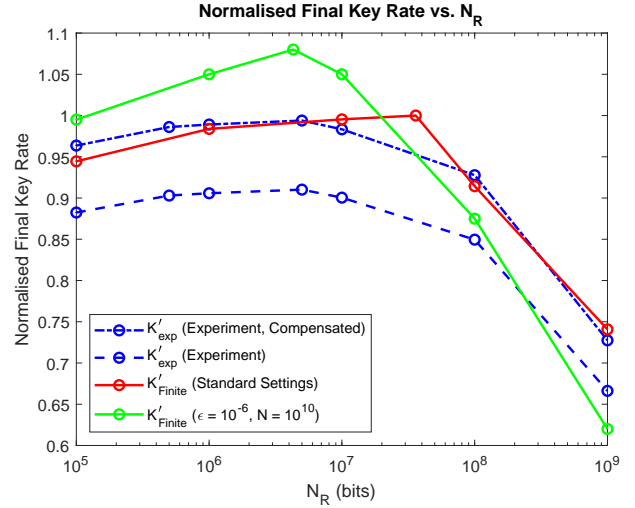


Fig. 6: Final Key Rate vs. LDPC Block Length. Here, we adopt the standard CV-QKD settings for the red and the blue curves. For the green curve, we adopt the following settings: $N = 10^{10}$, $m = 5$, $\epsilon_{EC} = 2\epsilon_s = \epsilon_{PA} = \epsilon_{PE} = 2.5 \times 10^{-7}$, $V_A = 4$, $T = 0.92$, $\xi_{ch} = 0.0180$ and $\xi_d = 0.0128$. We also set $c_h = 3.2 \times 10^{-9}$ seconds for the red and green curves. All the curves are normalised to the maximum of the red curve, i.e. $K'_{Finite} = 4.3 \times 10^5$ bits per second at $N_R = 3.6 \times 10^7$.

The optimal $N_R = 3.6 \times 10^7$ and 5×10^6 are found for K'_{Finite} and K'_{exp} , respectively. Assuming the usual practical scheme where N_R is simply selected randomly, our results for the standard CV-QKD settings show that using the optimal N_R for SR leads to a maximum gain of 33% on the final key rate. Other CV-QKD settings will provide different maximum gains. For example, the green curve of Fig. 6 provides for a 66% gain (not shown in the figure are the rates for $N_R > 10^9$). This point emphasises the need to consider the parameter settings before determining both the optimal N_R and the gain achieved relative to the standard practice of simply picking some $N_R < N$. Note that in our rate determinations, the normalisation of one in Fig. 6 corresponds to a key rate $K'_{Finite} = 4.3 \times 10^5$ bits per second, based on our hardware-specific value of $c_h = 3.2 \times 10^{-9}$ seconds.¹⁶ The reconciliation rate associated with this same key rate is 3.9×10^6 bits per second. Assuming the source rate of the quantum signalling was high enough (e.g. a 100MHz source), this reconciliation rate is higher than that required for delivery of secured ($\epsilon = 10^{-9}$) keys ($N = 10^9$) within flyover times (270 seconds) consistent with Micius-type orbits (see the introduction).

Comparing the two curves in Fig. 6, we find that there is still a small discrepancy between K'_{Finite} and K'_{exp} although they share a similar trend. The reason for such discrepancy is twofold. Firstly, there remain small trapping sets in the LDPC

¹⁶We adopted the following method to determine c_h . For m LDPC codes with $N_R = 10^6$ and $T = 0.9$, we obtained the total number of arithmetic operations for those codes. Next, we measured the elapsed time to reconcile a block of 10^6 quadrature values. We then obtained c_h by dividing the number of arithmetic operations to this measured elapsed time.

matrices.¹⁷ Although not part of our analysis (but included in the uncompensated curve of Fig. 6), we attempted to remove these trapping sets in our codes by using the algorithm of [58] so that fewer iterations will be used [59]. This reduced the number of decoding iterations by approximately 15% for $N_R = 10^6$ but did not remove the trapping sets completely. The remnant trapping sets inside the LDPC matrices lead to a larger number of decoding iterations than predicted by D_j . Determined by the Density Evolution Algorithm, D_j is a lower bound due to the assumption of cycle-free matrices and infinitely long block length [60]. Secondly, we note that selecting R_j so that $\sum_{j=0}^{m-1} R_j$ achieves C_{Finite} may lead to a p_{Decode} higher than the given ϵ_{EC} . In our experiment (and included in the shown results), we find that the K'_{exp} is 9% lower than the K'_{Finite} predicted by Eq. 22 due to the gap between $\sum_{j=0}^{m-1} R_j$ and C_{Finite} .

C. Final-key Effect for a Given N_o

In the satellite-based scenario, Alice and Bob starts the protocol with only N_o quantum signals because the satellite is only visible to the ground station for a limited time frame. In this section, we revisit the analysis of the final key rate in the finite-key regime and conduct a numerical search to show how the final key rate K is affected by N_e , for a given N_o and ϵ .

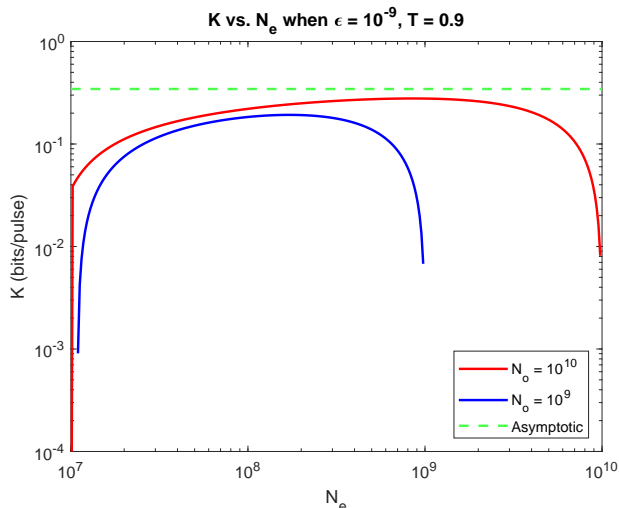


Fig. 7: K (in bits per pulse) vs. N_e when $N_o = 10^9$ (blue) and $N_o = 10^{10}$ (red). Here, we adopt the standard CV-QKD settings except that $N = 2(N_o - N_e)$ varies for different N_e .

In Fig. 7, we observe that K is cut off when N_e approaches 10^7 and 10^9 (for $N_o = 10^9$). At $N_e = 10^7$, the parameter confidence intervals are not consistent with a positive K . As N_e approaches N_o , K decreases rapidly since the number of quantum signals for reconciliation approaches zero. Similar remarks can also be applied for $N_o = 10^{10}$. In Fig. 7, we see that setting $N_e = \frac{N_o}{2}$ is an acceptable compromise between

accommodating finite-key effects and preserving enough quantum signals for the post-processing. In the appendix, we investigate varying N_e but where it is always constrained to $N_e = \frac{N_o}{2}$.

VI. DISCUSSION

We close our work with a brief discussion on recent developments in high-rate CV-QKD reconciliation via the massive parallelisation offered by GPUs and FPGAs. In [24], a GPU-based LDPC decoder was implemented, achieving a rate of 9×10^6 bits per second. In this implementation all GPU threads were used to minimise the decoding time of a *single* LDPC block of 2^{20} bits. In [61] and [62], the reconciliation rates were further increased to 3×10^7 and 6×10^7 bits per second, respectively, by simultaneously decoding *multiple* LDPC blocks of length 10^6 bits on a GPU. To our knowledge, the highest reconciliation rate obtained thus far is 2×10^8 bits per second - an outcome based on an FPGA [25]. All of these works show promise for the delivery of practical CV-QKD systems in which reconciliation does not become the bottleneck of the QKD process. However, none have introduced the type of optimisation we have introduced in this work and, therefore, all are likely candidates for further improvement in terms of the choice of the optimal block length. Based on our results we would anticipate this improvement to be significant for a wide range of CV-QKD parameter settings. Our work is also different from the above works in the following (less important) aspects.

- 1) *Reconciliation schemes for satellite-based CV-QKD.* High-speed implementations realised in [61], [62] have used multidimensional reconciliation [37]. This multidimensional scheme is preferred for low SNR - but not so for the higher SNRs available via the Gaussian post-selection technique - a technique likely to be more useful in the satellite context [1].
- 2) *Low probability of reconciliation failures.* In CV-QKD, Alice and Bob have to discard a block of reconciled bits if they detect a reconciliation failure (coding error) for that block. To compensate for the discarded bits, additional quantum signals need to be transmitted and reconciled, causing unwanted delays. Such delays can be problematic for satellite-based systems since the satellite is not always visible to the ground station. The FPGA-based reconciliation of [25] may suffer from this problem due to limited precision of arithmetic operations leading to higher reconciliation failures. As shown in many GPU-based works (including this work), GPU-based reconciliation offers less probability of reconciliation failure.

VII. CONCLUSION

In this work, we have carried out a full-blown analysis and experimental implementation of a Slice Reconciliation scheme applied to a specific CV QKD protocol (with post-selection) under simulated channel conditions anticipated for satellite-to-Earth channels. We have provided the optimal solution for the classical reconciliation process for this CV-QKD protocol in the context of massive parallelisation under the finite key regime. More specifically, we have identified the optimal block length when a large-code block is to be subdivided so as to

¹⁷These trapping sets are the primary reason that additional decoding iterations are consumed for only a marginal decrease of the decoding error, i.e. the error floor effect [58].

improve the final secure key rate in bits per second. Although our results were based on a specific CV-QKD protocol and a specific GPU architecture, the type of analysis we have introduced here will apply in general terms a large suite of CV-QKD protocols run over any form of architecture that offers massive parallelisation. Our results, therefore, pave the way to optimal reconciliation system design for a wide range of practical CV-QKD systems that operate in the finite key regime. As the demand on the finite key size grows (better security thresholds), and technology advances lead to larger quantum signalling rates, the importance of optimised multithreaded CV-QKD reconciliation will grow.

REFERENCES

- [1] N. Hosseini-dehaj, Z. Babar, R. Malaney, S. X. Ng, and L. Hanzo, "Satellite-Based Continuous-Variable Quantum Communications: State-of-the-Art and a Predictive Outlook," *IEEE Communications Surveys & Tutorials*, vol. 21, no. 1, 881–919, 2018.
- [2] C. H. Bennett and G. Brassard, "Quantum Cryptography: Public Key Distribution and Coin Tossing," in *Proceedings of IEEE International Conference on Computers, Systems and Signal Processing*, vol. 175, 8, 1984.
- [3] H. Weinfurter, "Quantum Communication Experiments with Discrete Variables," *Quantum Information: From Foundations to Quantum Technology Applications*, 369–381, 2016.
- [4] L. Gyöngyösi, L. Bacsardi, and S. Imre, "A Survey on Quantum Key Distribution," *Infocommunications Journal*, vol. 11, no. 2, 14–21, 2019.
- [5] S. Pirandola, U. L. Andersen, L. Banchi, M. Berta, D. Bunandar, R. Colbeck, D. Englund, T. Gehring, C. Lupo, C. Ottaviani, *et al.*, "Advances in Quantum Cryptography," *Advances in Optics and Photonics*, vol. 12, no. 4, 1012–1236, 2020.
- [6] B. Korzh, C. C. W. Lim, R. Houlmann, N. Gisin, M. J. Li, D. Nolan, B. Sanguinetti, R. Thew, and H. Zbinden, "Provably Secure and Practical Quantum Key Distribution over 307 km of Optical Fibre," *Nature Photonics*, vol. 9, no. 3, 163–168, 2015.
- [7] T. A. Eriksson, T. Hirano, B. J. Putnam, G. Rademacher, R. S. Luís, M. Fujiwara, R. Namiki, Y. Awaji, M. Takeoka, N. Wada, *et al.*, "Wavelength Division Multiplexing of Continuous Variable Quantum Key Distribution and 18.3 Tbit/s Data Channels," *Communications Physics*, vol. 2, no. 1, 1–8, 2019.
- [8] S.-Y. Shen, M.-W. Dai, X.-T. Zheng, Q.-Y. Sun, G.-C. Guo, and Z.-F. Han, "Free-Space Continuous-Variable Quantum Key Distribution of Unidimensional Gaussian Modulation Using Polarized Coherent States in an Urban Environment," *Physical Review A*, vol. 100, 012325, 2019.
- [9] L. Gyöngyösi and S. Imre, "Secret Key Rates of Free-Space Optical Continuous-Variable Quantum Key Distribution," *International Journal of Communication Systems*, vol. 32, no. 18, e4152, 2019.
- [10] P. Jouguet, S. Kunz-Jacques, and A. Leverrier, "Long-Distance Continuous-Variable Quantum Key Distribution with a Gaussian Modulation," *Physical Review A*, vol. 84, no. 6, 062317, 2011.
- [11] P. Jouguet, S. Kunz-Jacques, T. Debuisschert, S. Fossier, E. Diamanti, R. Alléaume, R. Tualle-Brouri, P. Grangier, A. Leverrier, P. Pache, *et al.*, "Field Test of Classical Symmetric Encryption with Continuous Variables Quantum Key Distribution," *Optics Express*, vol. 20, no. 13, 14030–14041, 2012.
- [12] Q. Liao, Y. Guo, D. Huang, P. Huang, and G. Zeng, "Long-Distance Continuous-Variable Quantum Key Distribution Using Non-Gaussian State-Discrimination Detection," *New Journal of Physics*, vol. 20, no. 2, 023015, 2018.
- [13] D. Guo, C. He, T. Guo, Z. Xue, Q. Feng, and J. Mu, "Comprehensive High-Speed Reconciliation for Continuous-Variable Quantum Key Distribution," *Quantum Information Processing*, vol. 19, no. 9, 1–19, 2020.
- [14] Y. Zhang, Z. Chen, S. Pirandola, X. Wang, C. Zhou, B. Chu, Y. Zhao, B. Xu, S. Yu, and H. Guo, "Long-Distance Continuous-Variable Quantum Key Distribution over 202.81 km of Fiber," *Physical Review Letters*, vol. 125, no. 1, 010502, 2020.
- [15] A. Leverrier, F. Grosshans, and P. Grangier, "Finite-Size Analysis of a Continuous-Variable Quantum Key Distribution," *Physical Review A*, vol. 81, no. 6, 062343, 2010.
- [16] F. Furrer, T. Franz, M. Berta, A. Leverrier, V. B. Scholz, M. Tomamichel, and R. F. Werner, "Continuous Variable Quantum Key Distribution: Finite-Key Analysis of Composable Security against Coherent Attacks," *Physical Review Letters*, vol. 109, no. 10, 100502, 2012.
- [17] S. Kish, E. Villaseñor, R. Malaney, K. Mudge, and K. Grant, "Feasibility Assessment for Practical Continuous Variable Quantum Key Distribution over the Satellite-to-Earth Channel," *Quantum Engineering*, vol. 2, no. 3, e50, 2020.
- [18] M. Tomamichel, C. C. W. Lim, N. Gisin, and R. Renner, "Tight Finite-Key Analysis for Quantum Cryptography," *Nature Communications*, vol. 3, no. 1, 1–6, 2012.
- [19] Z. Yuan, A. Plews, R. Takahashi, K. Doi, W. Tam, A. Sharpe, A. Dixon, E. Lavelle, J. Dynes, A. Murakami, *et al.*, "10-Mb/s Quantum Key Distribution," *Journal of Lightwave Technology*, vol. 36, no. 16, 3427–3433, 2018.
- [20] S.-K. Liao, W.-Q. Cai, W.-Y. Liu, L. Zhang, Y. Li, J.-G. Ren, J. Yin, Q. Shen, Y. Cao, Z.-P. Li, *et al.*, "Satellite-to-Ground Quantum Key Distribution," *Nature*, vol. 549, no. 7670, 43–47, 2017.
- [21] D. Lin, D. Huang, P. Huang, J. Peng, and G. Zeng, "High Performance Reconciliation for Continuous-Variable Quantum Key Distribution with LDPC Code," *International Journal of Quantum Information*, vol. 13, no. 02, 1550010, 2015.
- [22] X. Wang, Y. Zhang, S. Yu, B. Xu, Z. Li, and H. Guo, "Efficient Rate-Adaptive Reconciliation for Continuous-Variable Quantum Key Distribution," *Quantum Information & Computation*, vol. 17, no. 13–14, 1123–1134, 2017.
- [23] C. Zhou, X. Wang, Y. Zhang, Z. Zhang, S. Yu, and H. Guo, "Continuous-Variable Quantum Key Distribution with Rateless Reconciliation Protocol," *Physical Review Applied*, vol. 12, no. 5, 054013, 2019.
- [24] M. Milicevic, C. Feng, L. M. Zhang, and P. G. Gulak, "Quasi-Cyclic Multi-Edge LDPC Codes for Long-Distance Quantum Cryptography," *NPJ Quantum Information*, vol. 4, no. 1, 1–9, 2018.
- [25] S.-S. Yang, Z.-G. Lu, and Y.-M. Li, "High-Speed Post-Processing in Continuous-Variable Quantum Key Distribution Based on FPGA Implementation," *Journal of Lightwave Technology*, vol. 38, no. 15, 3935–3941, 2020.
- [26] H. Li and Y. Pang, "FPGA-Accelerated Quantum Computing Emulation and Quantum Key Distillation," *IEEE Micro*, vol. 41, no. 4, 49–57, 2021.
- [27] C. Weedbrook, A. M. Lance, W. P. Bowen, T. Symul, T. C. Ralph, and P. K. Lam, "Quantum Cryptography without Switching," *Physical Review Letters*, vol. 93, no. 17, 170504, 2004.
- [28] N. Hosseini-dehaj, A. M. Lance, T. Symul, N. Walk, and T. C. Ralph, "Finite-Size Effects in Continuous-Variable Quantum Key Distribution with Gaussian Postselection," *Physical Review A*, vol. 101, no. 5, 052335, 2020.
- [29] D. Dequal, L. T. Vidarte, V. R. Rodriguez, G. Vallone, P. Villoresi, A. Leverrier, and E. Diamanti, "Feasibility of Satellite-to-Ground Continuous-Variable Quantum Key Distribution," *NPJ Quantum Information*, vol. 7, no. 1, 1–10, 2020.
- [30] M. Bloch, A. Thangaraj, and S. W. McLaughlin, "Efficient Reconciliation of Correlated Continuous Random Variables Using LDPC Codes," *arXiv preprint cs/0509041*, 2005.
- [31] P. Jouguet, D. Elkouss, and S. Kunz-Jacques, "High-Bit-Rate Continuous-Variable Quantum Key Distribution," *Physical Review A*, vol. 90, no. 4, 042329, 2014.
- [32] H. Mani, T. Gehring, P. Grabenweger, B. Ömer, C. Pacher, and U. L. Andersen, "Multiedge-Type Low-Density Parity-Check Codes for Continuous-Variable Quantum Key Distribution," *Physical Review A*, vol. 103, no. 6, 062419, 2021.
- [33] H. Imai and S. Hirakawa, "A New Multilevel Coding Method Using Error-Correcting Codes," *IEEE Transactions on Information Theory*, vol. 23, no. 3, 371–377, 1977.
- [34] U. Wachsmann, R. F. Fischer, and J. B. Huber, "Multilevel codes: Theoretical concepts and practical design rules," *IEEE Transactions on Information Theory*, vol. 45, no. 5, 1361–1391, 1999.
- [35] R. D. Wesel, X. Liu, J. M. Cioffi, and C. Kominakis, "Constellation Labeling for Linear Encoders," *IEEE Transactions on Information Theory*, vol. 47, no. 6, 2417–2431, 2001.
- [36] M. Bloch, A. Thangaraj, S. W. McLaughlin, and J.-M. Merolla, "LDPC-Based Gaussian Key Reconciliation," in *IEEE Information Theory Workshop-ITW'06 Punta del Este*, 116–120, IEEE, 2006.
- [37] A. Leverrier, R. Alléaume, J. Boutros, G. Zémor, and P. Grangier, "Multidimensional Reconciliation for a Continuous-Variable Quantum Key Distribution," *Physical Review A*, vol. 77, no. 4, 042325, 2008.
- [38] J. Fiurášek and N. J. Cerf, "Gaussian Postselection and Virtual Noiseless Amplification in Continuous-Variable Quantum Key Distribution," *Physical Review A*, vol. 86, no. 6, 060302, 2012.

- [39] F. Darema, “The SPMD Model: Past, Present and Future,” in *European Parallel Virtual Machine/Message Passing Interface Users’ Group Meeting*, 1–1, Springer, 2001.
- [40] M. Pharr and W. R. Mark, “A SPMD Compiler for High-Performance CPU Programming,” in *Innovative Parallel Computing (InPar)*, 1–13, IEEE, 2012.
- [41] J. Lodewyck, M. Bloch, R. García-Patrón, S. Fossier, E. Karpov, E. Diamanti, T. Debuisschert, N. J. Cerf, R. Tualle-Brouri, S. W. McLaughlin, *et al.*, “Quantum Key Distribution over 25 km with an All-Fiber Continuous-Variable System,” *Physical Review A*, vol. 76, no. 4, 042305, 2007.
- [42] F. Laudenbach, C. Pacher, C.-H. F. Fung, A. Poppe, M. Peev, B. Schrenk, M. Hentschel, P. Walther, and H. Hübel, “Continuous-Variable Quantum Key Distribution with Gaussian Modulation—The Theory of Practical Implementations,” *Advanced Quantum Technologies*, vol. 1, no. 1, 1800011, 2018.
- [43] Y. Polyanskiy, H. V. Poor, and S. Verdú, “Channel Coding Rate in the Finite Blocklength Regime,” *IEEE Transactions on Information Theory*, vol. 56, no. 5, 2307–2359, 2010.
- [44] D. Slepian and J. Wolf, “Noiseless Coding of Correlated Information Sources,” *IEEE Transactions on Information Theory*, vol. 19, no. 4, 471–480, 1973.
- [45] T. Richardson and R. Urbanke, *Modern Coding Theory*. Cambridge University Press, 2008.
- [46] X. Ai, R. Malaney, and S. X. Ng, “A Reconciliation Strategy for Real-Time Satellite-Based QKD,” *IEEE Communications Letters*, vol. 24, no. 5, 1062–1066, 2020.
- [47] S.-Y. Chung, T. J. Richardson, and R. L. Urbanke, “Analysis of Sum-Product Decoding of Low-Density Parity-Check Codes Using a Gaussian Approximation,” *IEEE Transactions on Information Theory*, vol. 47, no. 2, 657–670, 2001.
- [48] V. A. Chandrasekhar and S. M. Aziz, “FPGA Implementation of an LDPC Decoder Using a Reduced Complexity Message Passing Algorithm,” *Journal of Networks*, vol. 6, no. 1, 36, 2011.
- [49] A. Leverrier, “Composable Security Proof for Continuous-Variable Quantum Key Distribution with Coherent States,” *Physical Review Letters*, vol. 114, no. 7, 070501, 2015.
- [50] C. Lupo, C. Ottaviani, P. Papanastasiou, and S. Pirandola, “Continuous-Variable Measurement-Device-Independent Quantum Key Distribution: Composable Security against Coherent Attacks,” *Physical Review A*, vol. 97, no. 5, 052327, 2018.
- [51] N. Hosseini-dehaj, N. Walk, and T. C. Ralph, “Optimal Realistic Attacks in Continuous-Variable Quantum Key Distribution,” *Physical Review A*, vol. 99, no. 5, 052336, 2019.
- [52] S. Pirandola, “Limits and Security of Free-Space Quantum Communications,” *Physical Review Research*, vol. 3, no. 1, 013279, 2021.
- [53] S. Pirandola, “Satellite Quantum Communications: Fundamental Bounds and Practical Security,” *Physical Review Research*, vol. 3, no. 2, 023130, 2021.
- [54] J. H. Mathews and K. D. Fink, *Numerical Methods Using MATLAB*, vol. 4. Pearson Prentice Hall Upper Saddle River, NJ, 2004.
- [55] A. Leverrier, “Security of Continuous-Variable Quantum Key Distribution via a Gaussian de Finetti Reduction,” *Physical Review Letters*, vol. 118, no. 20, 200501, 2017.
- [56] E. Villaseñor, R. Malaney, K. A. Mudge, and K. J. Grant, “Atmospheric Effects on Satellite-to-Ground Quantum Key Distribution Using Coherent States,” in *GLOBECOM 2020-2020 IEEE Global Communications Conference*, 1–6, IEEE, 2020.
- [57] J. Mateo, *Efficient Information Reconciliation for Quantum Key Distribution*. PhD thesis, Universidad Politécnica de Madrid, 2011.
- [58] T. Tian, C. R. Jones, J. D. Villasenor, and R. D. Wesel, “Selective Avoidance of Cycles in Irregular LDPC Code Construction,” *IEEE Transactions on Communications*, vol. 52, no. 8, 1242–1247, 2004.
- [59] D. V. Nguyen, S. K. Chilappagari, M. W. Marcellin, and B. Vasic, “On the Construction of Structured LDPC Codes Free of Small Trapping Sets,” *IEEE Transactions on Information Theory*, vol. 58, no. 4, 2280–2302, 2012.
- [60] S. Landner and O. Milenkovic, “Algorithmic and Combinatorial Analysis of Trapping Sets in Structured LDPC Codes,” in *International Conference on Wireless Networks, Communications and Mobile Computing*, vol. 1, 630–635, IEEE, 2005.
- [61] X. Wang, Y. Zhang, S. Yu, and H. Guo, “High Speed Error Correction for Continuous-Variable Quantum Key Distribution with Multi-Edge Type LDPC Code,” *Scientific Reports*, vol. 8, no. 1, 1–7, 2018.
- [62] Y. Li, X. Zhang, Y. Li, B. Xu, L. Ma, J. Yang, and W. Huang, “High-Throughput GPU Layered Decoder of Quasi-Cyclic Multi-Edge Type Low Density Parity Check Codes in Continuous-Variable Quantum Key Distribution Systems,” *Scientific Reports*, vol. 10, no. 1, 1–11, 2020.
- [63] F. Grosshans, “Collective Attacks and Unconditional Security in Continuous Variable Quantum Key Distribution,” *Physical Review Letters*, vol. 94, 020504, 2005.
- [64] M. Navascués, F. Grosshans, and A. Acín, “Optimality of Gaussian Attacks in Continuous-Variable Quantum Cryptography,” *Physical Review Letters*, vol. 97, no. 19, 190502, 2006.
- [65] S. Fossier, E. Diamanti, T. Debuisschert, R. Tualle-Brouri, and P. Grangier, “Improvement of Continuous-Variable Quantum Key Distribution Systems by Using Optical Preamplifiers,” *Journal of Physics B: Atomic, Molecular and Optical Physics*, vol. 42, no. 11, 114014, 2009.
- [66] P. Jouguet, S. Kunz-Jacques, E. Diamanti, and A. Leverrier, “Analysis of Imperfections in Practical Continuous-Variable Quantum Key Distribution,” *Physical Review A*, vol. 86, no. 3, 032309, 2012.

APPENDIX

In this appendix, we elaborate on the estimation of channel parameters, T and ξ_{ch} , from N_e quantum signals and determination of the upper bound of S_{BE}^{EFE} based on the estimated T and ξ_{ch} for a given N . Here, we closely follow the methodology in [17] (and references therein).

The parameter estimation at Step 4 of our protocol is a two-step process. Firstly, Alice and Bob estimate each coefficient in the covariance matrix between the shared states based on N_e (randomly selected) quantum signals sent from Bob. Then Alice uses these estimated coefficients to determine T and ξ_{ch} . In the asymptotic regime, the estimation of T and ξ_{ch} is exact since Alice and Bob use an infinite number of quantum signals. The following the two functions will be useful,

$$F_1(v_1, v_2) = \sqrt{\frac{v_1 + \sqrt{v_1^2 - 4v_2}}{2}}, \quad (33)$$

$$F_2(v_1, v_2) = \sqrt{\frac{v_1 - \sqrt{v_1^2 - 4v_2}}{2}}. \quad (34)$$

Alice can determine the Holevo Information between Bob and Eve’s states χ_{EB} via [63]–[65]

$$\chi_{EB} = \chi_E - \chi_{E|B}, \quad (35)$$

where χ_E is Eve’s von Neumann Entropy before Bob makes his heterodyne detection and $\chi_{E|B}$ is Eve’s von Neumann Entropy after his detection. The term χ_E is given by

$$\chi_E = Z \left(\frac{\psi_1 - 1}{2} \right) + Z \left(\frac{\psi_2 - 1}{2} \right), \quad (36)$$

where

$$Z(z) = (z + 1) \log(z + 1) - z \log z. \quad (37)$$

We define that $\psi_1 = F_1(\Psi_1, \Psi_2)$ and $\psi_2 = F_2(\Psi_1, \Psi_2)$ to be the symplectic eigenvalues of the covariance matrix of the shared states (before Bob’s heterodyne detection) where

$$\Psi_1 = (V_A + 1)^2(1 - 2T) + 2T + T^2(V_A + 1 + \chi_{ch}) \quad (38)$$

$$\Psi_2 = T^2((V_A + 1)\xi_{ch} + 1), \quad (39)$$

$$\chi_{ch} = \frac{1-T}{T} + \xi_{ch}. \quad (40)$$

The term $\chi_{E|B}$ is given by

$$\chi_{E|B} = Z \left(\frac{\theta_1 - 1}{2} \right) + Z \left(\frac{\theta_2 - 1}{2} \right) + Z \left(\frac{\theta_3 - 1}{2} \right), \quad (41)$$

where θ_1 , θ_2 and θ_3 are the symplectic eigenvalues of the covariance matrix of the shared states (after Bob’s heterodyne

detection). Specifically, we have $\theta_1 = F_1(\Theta_1, \Theta_2)$ and $\theta_2 = F_2(\Theta_1, \Theta_2)$ where

$$\Theta_1 = \left(\Psi_1 \chi_d^2 + \Psi_2 + 1 + 2\chi_d \left(T(V_A + 1 + \chi_{ch}) + (V_A + 1) \sqrt{\Psi_2} \right) + 2T(V_A^2 + 2V_A) \right) \frac{1}{T^2(V_A + 1 + \chi)}, \quad (42)$$

$$\Theta_2 = \left(\frac{V_A + 1 + \chi_d \sqrt{\Psi_2}}{T(V_A + 1 + \chi)} \right)^2, \quad (43)$$

$$\chi_d = \frac{2 - \eta_d}{\eta_d} + \frac{2\chi_d}{\eta_d}, \quad (44)$$

$$\chi = \chi_{ch} + \frac{\chi_d}{T}, \quad (45)$$

where η_d is the detection efficiency and we set $\eta_d = 1$ for simplicity. It is known that $\theta_3 = 1$ under the assumption of Gaussian collective attack [65]. Therefore, we have $Z\left(\frac{\theta_3 - 1}{2}\right) = 0$.

However, the estimation of T and ξ_{ch} is not exact in the finite-key regime. The estimated T and ξ_{ch} are subject to statistical fluctuations that leads to a deviation of the estimated T and ξ_{ch} from their true values (since Alice and Bob use only N_e signals for the estimation at Step 4). The impact of using a finite number of quantum signals for parameter estimation in the security analysis is twofold. Firstly, the protocol will fail with a probability of ϵ_{PE} if the true value of T or ξ_{ch} is out of the confidence interval set by that ϵ_{PE} . Secondly, the amount of the deviation of the estimated T and ξ_{ch} from their true values is probabilistic. The lower and upper limits of the confidence interval of the estimated T for a given ϵ_{PE} are given by [15], [66]

$$T^L = \left(\hat{t} - \tau_{\epsilon_{PE}/2} \sqrt{\frac{\hat{\sigma}^2}{N_e V_A}} \right)^2, \quad (46)$$

$$T^U = \left(\hat{t} + \tau_{\epsilon_{PE}/2} \sqrt{\frac{\hat{\sigma}^2}{N_e V_A}} \right)^2, \quad (47)$$

where $\tau_{\epsilon_{PE}/2} = Q^{-1}\left(\frac{\epsilon_{PE}}{2}\right)$; and \hat{t} and $\hat{\sigma}$ are the estimators for T and ξ_{ch} , respectively. Similarly, the lower and upper limits of the confidence interval of the estimated ξ_{ch} for a given ϵ_{PE} are given by [15], [66]

$$\xi_{ch}^L = \frac{\hat{\sigma}^2 - \tau_{\epsilon_{PE}/2} \frac{\hat{\sigma}^2 \sqrt{2}}{\sqrt{N_e}} + 1 + \xi_d}{\hat{t}^2}, \quad (48)$$

$$\xi_{ch}^U = \frac{\hat{\sigma}^2 + \tau_{\epsilon_{PE}/2} \frac{\hat{\sigma}^2 \sqrt{2}}{\sqrt{N_e}} - 1 - \xi_d}{\hat{t}^2}, \quad (49)$$

respectively.

Based on the above, we can now determine $S_{BE}^{\epsilon_{PE}}$, i.e. the upper bound of χ_{BE} in the finite-key regime. Firstly, for the purpose of analysis, we set the expectation of \hat{t} and $\hat{\sigma}$ as $\sqrt{\eta_d T}$ and $T\eta_d \xi_{ch} + 1 + \xi_d$, respectively. Then, we replace T and ξ_{ch} in Eqs. 38 to 40 and Eqs. 42 to 45 with T^L and ξ_{ch}^U , respectively. Next, we determine $S_{BE}^{\epsilon_{PE}}$ by using Eqs. 33, 34 to determine all the symplectic eigenvalues. Finally, we use Eq. 36, 41 and 35 to obtain $S_{BE}^{\epsilon_{PE}}$.

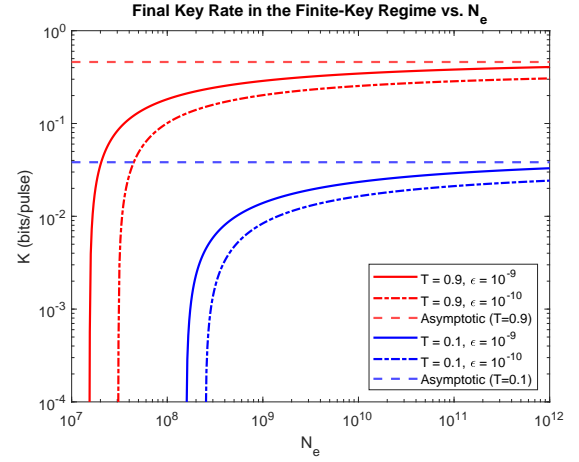


Fig. 8: K (in bits per pulse) vs. N_e . Here we adopt the standard CV-QKD setting except for N_o for all the curves. For all the curves, we assume $N_e = \frac{N_o}{2}$.

The motivation of setting a large N_e is to reduce the length of the confidence intervals when estimating T and ξ_{ch} . In Fig. 8, we compare the impact on K when setting different N_e . For all the curves in Fig. 8, we assume $N_e = \frac{N_o}{2}$ (see Section V-C for the case of varying N_e for a given N_o). The “take-away” message is that, for a given ϵ , setting a large N_e is necessary for most CV-QKD deployments if a significant reduction of K is to be avoided.